ELSEVIER

Chemical Engineering Journal 137 (2008) 45–53

Chemical Engineering Journal

www.elsevier.com/locate/cej

Synthesis and stealthing study of bare and PEGylated silica micro- and nanoparticles as potential drug-delivery vectors

Clara Yagüe, María Moros, Valeria Grazú, Manuel Arruebo *, Jesús Santamaría

Department of Chemical and Environmental Engineering and Aragon Nanoscience Institute, University of Zaragoza, 50009 Zaragoza, Spain

Received 30 May 2007; received in revised form 25 July 2007; accepted 26 July 2007

Abstract

Bare and PEGylated silica spheres have been synthesized and characterized in order to study their potential application as intravenous drug-delivery vectors. Solubility under physiological conditions (in simulated body fluid) as well as standard protein adsorption experiments (immobilization of bovine serum albumin, BSA) were carried out in order to analyze the stability and the potential avoidance of the reticuloendothelial system (RES) achieved after PEGylation. The influences of the chain length of the PEG, as well as, of the temperature in the esterification reaction were also analyzed.

Keywords: Silica particles; Drug delivery; Pegylation; MCM-41; MCM-48; Biodegradability; BSA adsorption; PEG

1. Introduction

Different organic materials such as polymeric nanoparticles, liposomes and micelles have been studied as drug-delivery vectors. In contrast, inorganic materials have been less studied as carriers of drugs and bio-active molecules (including gene delivery) in spite of important advantages such as mechanical stability and low toxicity compared to some cationic carriers (lipids and polymers) [1]. Among inorganic materials, silica offers an attractive alternative to polymeric micro- and nanoparticles both biodegradable (i.e., polyesters, poly(DL-lactide-co-glycolide) and non-biodegradable (i.e., 3-hydroxypropyl methacrylate). Thus, the use of silica has been advocated on account of its low toxicity and biocompatibility, its high chemical and mechanical stability, and its hydrophilic character and porous structure that can, in principle, be tailored to control the diffusion rate of an adsorbed or encapsulated drug. Silica does not swell nor change its porosity with variations in pH, and it is not vulnerable to microbiological attack [2].

For biomedical applications involving intravenous administration of micro- and nanoparticles, biodegradability, size and surface characteristics are the most important parameters regarding the ultimate fate and distribution of the particles in the body.

1.1. Biodegradability

Calcined silica is considered non-biodegradable, but sol–gel derived silica xerogels ($SiO_2{\cdot}nH_2O$) with pores ranging typically between 1 and 10 nm in diameter have been reported to biodegrade and eventually dissolve [3]. Therefore, they have been used as carrier materials for implantable controlled drug-delivery systems [4]. It has been reported that after subcutaneous administration in mice, silica xerogels cause no adverse tissue reactions and degrade in the body to $Si(OH)_4$, which is eliminated through the kidneys [5]. In spite of its very low biodegradability, silica has been used for *in vivo* applications. Thus, for instance, silica nanoparticles (∼30 nm) have been used as drug carriers in photodynamic therapy on tumour cells [6]. Also, injectable silica nanoparticles (<100 nm) encapsulating enzymes have been synthesized showing higher stability towards temperature and pH compared to free enzyme molecules [7]. The chemical stability and porous structure of silica have been widely used to prevent gene degradation in transfection applications using the silica particle as a carrier for gene delivery and as a matrix for enzyme immobilization [8].

1.2. Size

For non-biodegradable nanoparticles, the maximum size for intravenous administration is determined by the spleen cut-off. Since the spleen filters the blood removing foreign particles

* Corresponding author. Tel.: +34 976 761000x3514; fax: +34 976 762142.
E-mail address: arruebom@unizar.es (M. Arruebo).

1385-8947/$ – see front matter © 2007 Elsevier B.V. All rights reserved.
doi:10.1016/j.cej.2007.07.088

larger than 200 nm [9] particles above this size have a short life in the bloodstream and therefore a low efficiency as drug carriers.

In addition, for biodegradable particles, the glomerular excretion by the kidneys can be avoided by using nanoparticles with a larger size than its threshold value (42–50 kDa for water-soluble polymers, reaching values as high as 100 kDa for dendrimers [10]); therefore, the size can be tailored to obtain long-circulation nanoparticles (i.e., liposomes) which avoid fast clearance [11]. In passive targeting, the size of the nanoparticles is designed to extravasate from the circulatory system into the interstitial fluid to reach the target cells based on the enhanced permeation and retention (EPR) effect [12]. The majority of solid tumours exhibit a vascular pore cut-off size between 380 and 780 nm, although vasculature organization may differ depending on the tumour type, its growth rate and, microenvironment [13]. Hence, there is an optimal size of the biodegradable particles to obtain maximum accumulation at the target using the natural permeability of the capillary, while for non-biodegradable particles the size is going to be limited by the glomerular filtration rate. Particles larger than that threshold will be accumulated in the different organs of the RES, principally the liver, spleen and bone marrow.

Silica particles are generally prepared following the sol–gel procedure proposed by Stöber et al. [14]. Other methods such as reverse microemulsion or water in oil emulsion have been also used in order to control the size of the particles obtained. The obtained silica using the sol–gel procedure is dense and/or microporous with moderate surface area values [15]. In order to obtain mesoporous (2 nm < pore size < 50 nm) silica of high surface area, different amphiphilic molecules (surfactants) are added to the solution. Ionic (cationic and anionic) surfactants direct the mesophase formation based on the electrostatic interactions and neutral surfactants direct the synthesis probably by hydrogen-bonding interactions. Cetyl trimethylammonium bromide (CTABr) is the most commonly used cationic surfactant in the synthesis of mesoporous silica. Depending on the concentration of the surfactant added and the synthesis temperature, hydrolyzed silicon alkoxides reorganize to form micelles (above the critical micelle concentration), hexagonal ordered arrays (MCM-41), cubic ordered arrays (MCM-48) or lamellar structures (MCM-50). Both the method to produce dense/microporous (without surfactant added) silica particles and the method to produce mesoporous (with surfactant added) silica particles can be controlled to prepare nanoparticles with sizes as low as 50 nm [16] (for the surfactant-free synthesis) and 15 nm (with CTABr as surfactant) [17]. Several review papers have been published, dealing with different aspects and chemical strategies to synthesize and design nanostructured materials [18].

1.3. Surface characteristics

Neutral charge and hydrophilicity are desired surface characteristic of the nanoparticles in order to avoid the rapid uptake by monocytes and consequently by organ-resident phagocytic cells (i.e., Kupffer cells in the liver). Most of the strategies to reach those requirements use hydrophilic polymers (i.e., poly(ethylene glycol), PEG) that, in addition, show steric effects which help to stabilize the nanoparticles preventing agglomeration. PEG has been bound to silica through direct surface esterification of its surface hydroxyl groups and the silica surface silanols or through a urethane linkage in order to stabilize colloidal silica in water [18]. In some cases, poly(ethylene glycol) is attached to the external surface of the silica particles by means of hydrogen bonding, in other cases the synthesis of the silica particles takes place directly in the presence of PEG rendering ester linkages (Si–O–C).

Hydrogen bonding between the silica surface hydroxyl groups and nearby silica particles produces agglomeration [19]. Agglomeration may also occur through the condensation of silanol groups on the surface of individual particles [20]. There are three kinds of silanols on the silica surface: terminal (isolated) silanols (one hydroxyl group attached to a Si atom on the surface), geminal silanols (two hydroxyl groups attached) and ethereal silanols (forming a siloxane bond Si–O–Si) [21]. Dehydration by calcination eliminates silanol groups so that particle aggregation becomes less likely [22]; however, hydrogen bonding still occurs, and calcination may also have undesired effects such as a reduction in the hydrophilic character of the silica and in the amount of surface hydroxyl groups which are susceptible to be functionalizated.

In this work, we have investigated the effect of different synthesis variables on the final size of silica particles prepared by a sol–gel procedure. Some of these silica particles have been PEGylated with PEG of different molecular sizes to study the effect of PEG on the stability of the suspension. In order to try to improve the hydrophilicity and biodegradability of the silica particles, the removal of the template was carried out by extraction with alcoholic solutions of ammonium nitrate as an alternative to the standard calcination procedures. The electrostatic stabilization of the silica dispersion was also studied at different pH levels for both bare and PEGylated silica particles. Finally, protein adsorption experiments were carried out to gain some insight on the potential stealthing effect of PEG grafting on silica particles.

2. Experimental

2.1. Sol–gel synthesis of mesoporous and PEGylated silica particles

Two different synthesis procedures have been followed in order to obtain mesoporous silica particles: (i) the work of Zeng et al. [23] which describes the synthesis of MCM-41 microparticles (named A hereafter) using a precursor gel with the following molar composition: 1 TEOS:0.035 CTABr:0.0175 NaOH:692.5 H_2O and by stirring at 353 K for 3 h, and (ii) the work of Lebedev et al. [24] which shows the synthesis of mesoporous spherical silica microparticles with two structures: cubic MCM-48 in the central part and hexagonal MCM-41 in the outer part (particles named B hereafter) by using a precursor gel with the following molar composition: 1 TEOS:0.03 CTABr:11 NH_3:58 EtOH:144 H_2O and by stirring for 2 h at room temperature. For the latter, we have studied the influence of different synthesis parameters

in the final size of the obtained particles. The removal of the surfactant was carried out either by calcination (according to the reference [24]) or by extraction, dispersing the silica particles (∼1 wt.%) in a 0.03 M ammonium nitrate solution in ethanol and stirring the mixture at 60 °C for 1 h. After extraction, the powders were recovered by filtration and washed with ethanol and deionized water. This treatment was repeated twice.

Sigma–Aldrich (St. Louis, MO, USA) supplied the chemical reagents used in the three synthesis described which include tetraethyl orthosilicate (TEOS, 98 wt.%), tetramethyl orthosilicate (TMOS, 98 wt.%), cetyltrimethyl-ammonium bromide (CTABr, 99.3 wt.%), aqueous ammonia (28–30 wt.%) and ethanol.

The synthesis of PEGylated dense silica particles (named C hereafter) was carried out following the synthesis procedure described by Xu et al. [25]. The method can be summarized as follows: the different molecular weigh polymers tested are dissolved in a mixed solution of ammonium hydroxide and methanol in a first step. TMOS (the silica source) is added dropwise and after stirring for 4 h, the samples are collected and washed with ethanol. It is important to point out that the synthesis is surfactant-free. Sigma–Aldrich supplied poly(ethylene glycol) of different molecular weights (3000, 6000 and 35,000 g/mol).

2.2. Characterization of the silica particles

Physicochemical characterization of the samples was carried out by means of scanning electron microscopy with energy dispersive X-ray analysis (SEM-EDX), photon correlation spectroscopy (PCS), N_2 adsorption isotherms, Fourier transform infrared spectroscopy (FTIR), thermogravimetric analysis (TGA) and X-ray powder diffraction at low diffraction angles (XRD). BET surface areas, N_2 adsorption/desorption isotherms and pore-size distributions were obtained on a Micromeritics ASAP 2020 V1 device at 77 K. The pore-size distribution of the silica particles was calculated using the desorption branch of the N_2 adsorption/desorption isotherm with the Barret-Joyner-Halenda (BJH) method. The micropore volume of the samples was calculated from the *t*-plot method. The particle-size distribution and zeta potential of the dispersed materials were obtained by photon correlation spectroscopy (PCS) measurements (Malvern Zetasizer 3000 HS). X-ray powder diffraction at low diffraction angles was performed on a Bruker D-advance diffractometer equipped with a GADDS area detector using filtered Cu Kα radiation. The samples were also examined by scanning electron microscopy (SEM) in a JEOL JSM-6400 instrument operating at 3–20 kV, where energy dispersive X-ray spectroscopy (EDS) analysis was also carried out. Thermogravimetric analysis (TGA) was performed using a Mettler-Toledo equipment (TGA/DTA 851e SF/1100 °C). The mass loss during the treatment was measured with N_2 as purge gas, from 25 to 600 °C with 0.1 °C/min heating and cooling rates. Pure air was used to burn out the PEG in order to evaluate the amount of polymer on the silica particles under the same heating/cooling conditions. The sample holder was a ceramic alumina crucible of 70 μL of volume.

2.3. Dissolution tests

Simulated body fluid (SBF, pH 7.4) was prepared by mixing in distilled and deionized water reagent grade NaCl, $NaHCO_3$, KCl, $K_2HPO_4{\cdot}3H_2O$, $MgCl_2{\cdot}6H_2O$, HCl, $CaCl_2$, Na_2SO_4 and $NH_2C(CH_2OH)_3$ (all the chemicals were supplied by Sigma–Aldrich) according to procedures described in the literature [26]. The solution was kept at 37 °C and the pH was maintained at 7.3–7.4. A 75 mg silica powder were pressed into a disc and soaked in 250 mL of the previously prepared SBF while continuously stirring the dispersion in order to minimize external diffusion limitations. The dissolution of silica to the fluid was measured by UV–vis spectrophotometry analyzing the silicon released by photometric determination as silico-molybdenum blue using Standard Test NANOCOLOR® Silica (Macherey-Nagel GmbH & Co., Germany). It is important to point out that this test only measures ionic silicon and not solid silica. FTIR data were obtained using a Mattson Research Series spectrometer in air at room temperature. The solids were homogeneously dispersed in KBr (2 wt.% approximately) and pressed into discs. The spectra were recorded with a resolution of 4 cm^{-1} and 80 scans per spectrum.

2.4. Standard BSA adsorption assay

Adsorption of bovine serum albumin (BSA), purchased from Sigma–Aldrich, was carried out by mixing 10 mg of the particles to be tested with 1 mL of BSA solution of a certain concentration. The mixtures were gently agitated at 37 °C in an orbital shaker. Periodically, samples of supernatants were taken and protein concentration analyzed according to the bicinchoninic acid (purchased from Pierce, Rockford, IL, USA) (BCA) assay [27]. The amount of bound BSA was calculated by mass balance as the difference between the amount of protein added and the amount of unbound protein, measured spectrophotometrically. Each adsorption experiment was performed at least three times.

The effect of pH on adsorption was evaluated using a 70 μg/mL BSA solution prepared in 10 mM sodium acetate/acetic acid buffer at pH 4.7 or in 10 mM sodium phosphate buffer at pH 7.4.

To evaluate the maximum protein-binding capacity of the different synthesized particles, different BSA solutions prepared in sodium buffered saline solution at pH 7.4 (PBS) with a protein concentration in the range of 15–700 μg/ml were used.

The influence of the temperature and the molecular weight of PEG used in the synthesis of Type C nanoparticles were evaluated using a BSA solution of 70 μg/mL prepared in PBS at pH 7.4.

3. Results and discussion

3.1. Particles structural characterization

The results of the structural characterization of the three kinds of silica particles synthesized in this work are shown in Table 1.

For the Type A silica particles, the XRD results showed the characteristic diffraction caused by the ordering in the meso-

Table 1
Characterization of the silica particles synthesized in this work

Silica particles	BET surface area (m^2/g)	BJH pore size (nm)	BJH pore volume (cm^3/g)	Structure	Average particle size (nm)[a]	Hydrodynamic particle size in water (nm)[b]	Hydrodynamic particle size in PBS at pH 7.4 (nm)[b]
A	1305 ± 44	3.0	0.89	MCM-41	130 ± 20	254 ± 120	371 ± 65
B	927 ± 1	2.7	0.76	MCM-48	540 ± 200	1858 ± 429	1360 ± 109
C PEG 3000 g/mol	77 ± 1	–	0.32[c]	Amorphous	155 ± 20	261 ± 27	151 ± 23
C PEG 6000 g/mol	–	–	–	Amorphous	200 ± 20	216 ± 66	271 ± 25
C PEG 35,000 g/mol	–	–	–	Amorphous	210 ± 20	236 ± 78	253 ± 22

[a] Statistical analysis using SEM photographs.
[b] Dynamic light scattering results.
[c] Pore volume due to intra-particle spaces.

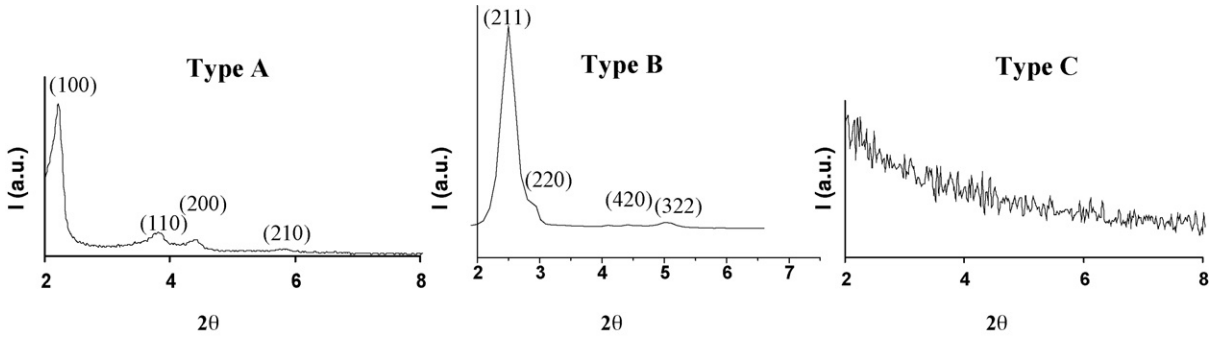

Fig. 1. X-ray powder diffraction patterns for the three kinds of silica particles synthesized in this work. Types A, B and C synthesized according to the experimental procedures described in references [23–25], respectively.

porous MCM-41 (*P6mm* symmetry group). The as-synthesized samples exhibit a marked (1 0 0) peak with weaker reflections corresponding to the (1 1 0) and (2 0 0) diffractions (Fig. 1), characteristic of MCM-41 materials [24]. The hydrodynamic diameter measured using dynamic light scattering revealed inter-particle agglomeration in all cases, probably due to hydrogen bonding between the hydroxyl surface groups of the silica. For the Type B silica particles, the characteristic diffraction peaks of the MCM-48 cubic structure (*Ia3d* symmetry) were obtained, in agreement with the results showed by Lebedev et al. [24]. Both A and B types of silica particles showed type IV adsorption isotherms characteristic of mesoporous materials (Fig. 2). For the A and B types, the micropore volume (calculated from the *t*-plot method) was nearly zero. The high surface areas obtained for the mesoporous silica particles make them attractive for drug-delivery applications. Type C silica particles showed the characteristic XRD pattern of amorphous samples (Fig. 1). While some agglomeration still exists in this case, the results of Table 1 clearly show that the poly(ethylene glycol) coating strongly reduces the silica agglomeration compared to the Types A and B silica particles, especially in PBS solution, where agglomeration is practically eliminated. Those Type C particles showed a Type II adsorption isotherm characteristic of dense solids where only macropores are present, corresponding to intraparticle spaces (with a Gaussian particle size distribution centred at 42 nm). For that sample, the PEG coating was removed by calcination from the PEGylated silica particles before the N_2 adsorption experiment. A H4 hysteresis loop was observed for that sample in a P/P_0 range of 0.9–1 which is associated with the filling and emptying of the macroporous voids between silica particles by capillary condensation.

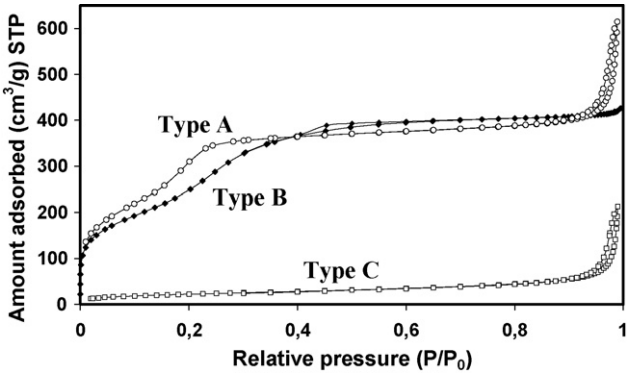

Fig. 2. . N_2 adsorption/desorption isotherms for the three kinds of silica particles synthesized in this work. Type C silica particles were synthesized using PEG of 3000 g/mol.

3.2. Controlling the silica particle size

For biodegradable particles many references in the literature describe microparticles with sizes of several hundreds of nanometres used for intravenous applications based mainly on polyesters (i.e., PLA or PLGA). For non-biodegradable nanoparticles, their sizes should be at least smaller than the spleen filtration cut-off (200 nm) [9], and to avoid bioaccumulation, the particle must have a molecular weight sufficiently low to allow renal elimination [28].

In order to control the particle size of the silica particles prepared in this work, we studied the influence of different

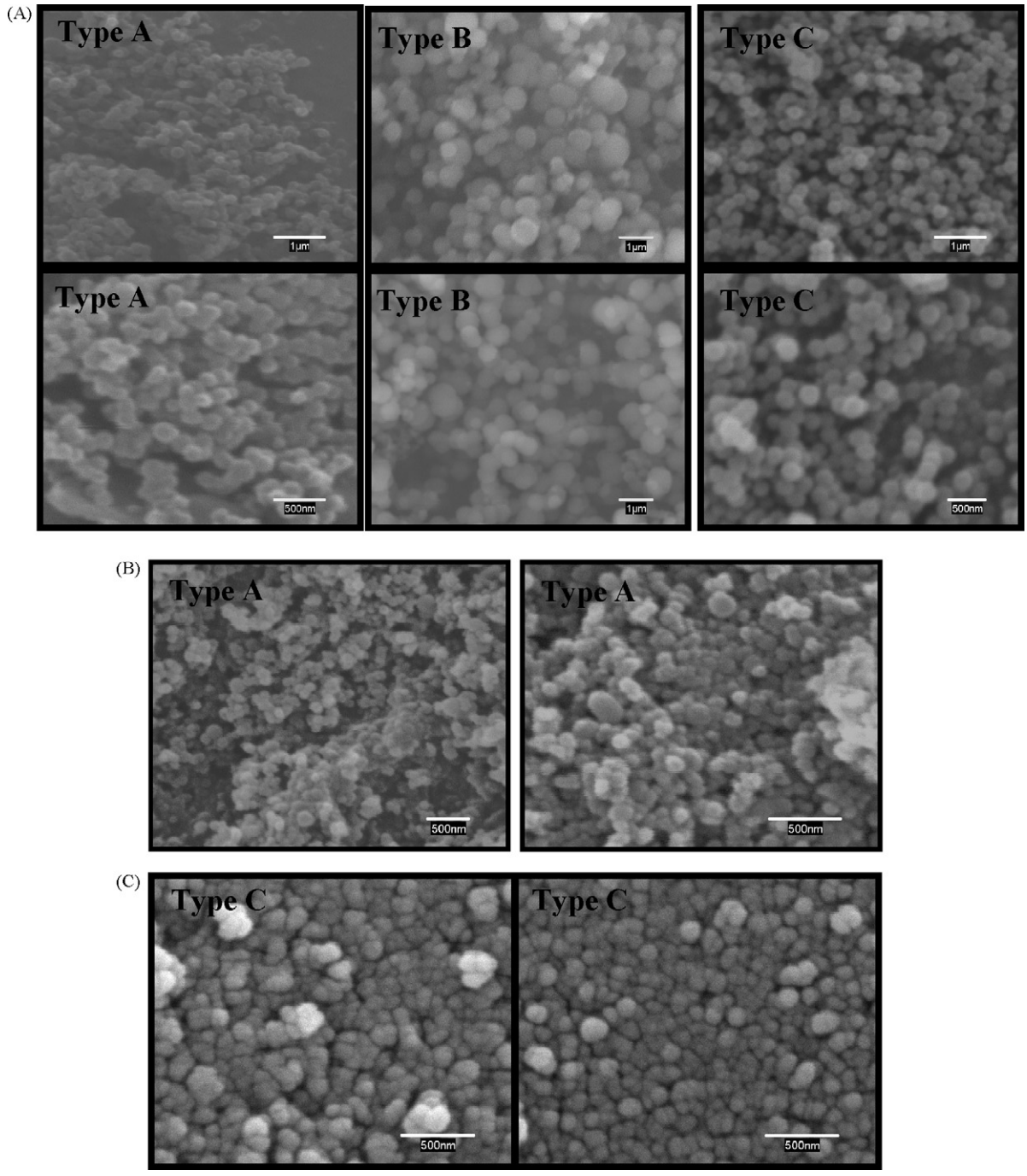

Fig. 3. (A) SEM photographs describing the morphological structure of the silica particles prepared in this work. (B) The smallest type A silica nanoparticles with sizes as small as 70 ± 10 nm. (C) PEGylated silica nanoparticles (Type C) with a diameter of 80 ± 20 nm.

parameters in the synthesis of the Type B silica particles. We assume that similar effects would be obtained for A and C type silicas, since comparable sol–gel procedures were used. Fig. 3 shows the morphological characteristics of the three kinds of silica particles. EDS analysis did not reveal the presence of any other atoms besides Si and O.

For the Type B particles, the following variables were studied: amount of TEOS and ammonia (catalyst) added, type of alcohol (methanol and ethanol were used with different polarity and molecular weight), length of the aliphatic chain of the surfactant (cetyltrimethylammonium bromide (CTABr) and dodecyltrimethylammonium bromide (DTABr), with 16 and 12 carbon atoms, respectively, were used), stirring speed, and pH (in the range 10.5–12.7). While a full study has not been carried out, the results obtained are sufficient, in some cases, to illustrate trends. Each of the synthesis was repeated three times in order to assure the reproducibility of the results. The average particle sizes were obtained from statistical analysis ($N = 50$) carried out on the SEM photographs taken on calcined samples.

The results indicate that the stirring speed, the pH (within the range studied), and the size of the surfactant molecule do not seem have an important effect regarding the size of the

Table 2
Ratio of the areas under the curve for the FTIR peaks obtained at 1700 cm^{-1} (corresponding to the Si–OH stretching bond) and at 1100 cm^{-1} (corresponding to the Si–O–Si bonds)

Area ratio $Si–OH_{stretching}/Si–O–Si$	Type A before surfactant removal	Type A surfactant removed by calcination	Type A surfactant removed by extraction	Type B surfactant removed by calcination	Type C[a] surfactant-free synthesis
$I_{1700(cm^{-1})}/I_{1100(cm^{-1})}$	0.306	0.204	0.259	0.128	0.247

[a] PEG 3000 g/mol.

particles synthesized. The particles obtained at low stirring speed (300 rpm) had an average particle size of 480 ± 150 nm, versus 540 ± 200 nm at high speed (1500 rpm); in addition, following the original preparation procedure [24], and by synthesizing under sonication the obtained average particle size was 500 ± 140 nm. This suggests that, even at the lowest agitation tested, the rate of supply of nutrients from the solution to the growing particles is sufficiently high and therefore the process is not mass-transfer limited. Similarly, within the range studied (10.5–12.7) the pH did not appear to have any statistically significant influence on the obtained particle sizes (results not shown).

Regarding the size of the surfactant molecules, using a surfactant with an aliphatic chain of 12 atoms of carbon, resulted in particle sizes of 430 ± 150 nm somewhat smaller but with a size distribution strongly overlapping with the original 540 ± 200 nm obtained with CTABr (C16) as surfactant. In contrast, the surfactant size did have a strong effect on the particle pore size, with smaller surfactants giving rise to lower diameter mesopores, as could be expected. Thus, with CTABr and DTABr as surfactants the obtained particle-pore sizes showed an average distribution of 2.7 and 2.0 nm, respectively.

Other changes that led to a decrease in the mean particle size were: (i) an increase in the amount of catalyst (adding a 100 wt.% increase in its concentration reduced particle sizes from 540 ± 200 to 360 ± 100 nm compared to the original recipe); (ii) replacement of ethanol by methanol (with a higher polarity and a smaller size) as the solvent alcohol (from 540 ± 200 nm with ethanol to 380 ± 110 nm with methanol); (iii) decreasing the amount of TEOS (a 50 wt.% decrease in the amount added to the reaction vessel reduced particle size from 540 ± 200 to 340 ± 70 nm).

In conclusion, the most important parameters regarding control of the particle size of silica particles prepared by the sol–gel process seem to be the concentration of the silica source (or the ratio silica source/water), the polarity of the alcohol, and the amount of the catalyst added. Those results are in general agreement with several works published in the literature [25,29,30].

The smallest Type A silica nanoparticles in this work were obtained using a diluted solution of CTAB 2.7 mM in water and a mixed solution of TMOS 0.56 M in methanol, at 60 °C, and adding a few drops of NH_3 (approximately 1 mL, 30 wt.%). This yielded silica particles as small as 70 ± 10 nm (see Fig. 3B).

For the surfactant-free synthesis, PEGylated silica nanoparticles (Type C) with a diameter of 80 ± 20 nm could be obtained by reducing the concentration of TMOS used during the synthesis, and with 100 wt.% in excess methanol as co-solvent (Fig. 3C).

3.3. Surface characterization

After synthesis, it is necessary to remove the surfactant and release the mesoporous structure, a process normally carried out by calcination. However, calcination at high temperatures strongly reduces the amount of surface hydroxyl groups on silica particles because of the condensation of the silanol groups [22]. In this work, we have carried out the removal of the surfactant by calcination and by extraction, and we have compared the populations of surface groups after these processes using FTIR. The complete removal of the surfactant was assessed by observing the complete extinction of the characteristic FTIR peaks at 2850 and 2930 cm^{-1} corresponding to the distinctive bonds of the surfactant (CTABr). The removal of the surfactant was also corroborated by thermogravimetric analysis (results not shown).

Table 2 shows the FTIR integrated area intensity ratio of the Si–OH stretching bond with respect to the Si–O–Si bond for different samples and treatments. All the samples were dried in a vacuum oven before each measurement. Clearly, the amount of OH groups remaining after extraction is considerably higher, showing the efficiency of extraction in reducing the loss of surface hydroxyl groups during surfactant removal. On the other hand, it can also be observed that poly(ethylene glycol) coated silica particles display a highly hydrophilic surface compared to the bare silica after calcination. The amount of PEG on the resulting PEGylated silica particles was 5.8, 3.0 and 5.6 wt.% for the 3000, 6000 and 35,000 g/mol PEG, respectively, as calculated from thermogravimetric analysis.

3.4. Solubility in SBF

To evaluate the influence of the different synthesis procedures, and of the amount of surface hydroxyl groups on particle solubility, the samples were immersed in SBF and the amount of silicon dissolved was analyzed by means of UV–vis spectrophotometry. The results (Fig. 4) show that the three kinds of silica particles synthesized in this work present a similar dissolution pattern, with a faster initial period where the most readily soluble fractions are incorporated into the SBF, followed by a slower dissolution process. The silica dissolution can be attributed to the hydrolysis of the siloxane bonds to render silicic acid, and the low rate of dissolution observed stems from the high chemical stability of Si–O–Si bonds. In our case, after 200 h the maximum concentration of dissolved silica was 45 ppm, far from saturation which would be reached at around 116 ppm [31]. In addition, Fig. 4 allows to compare the evolution of the dissolution patterns for Type A silica particles where different procedures (extraction and calcination) were used to remove the surfactant. It can be

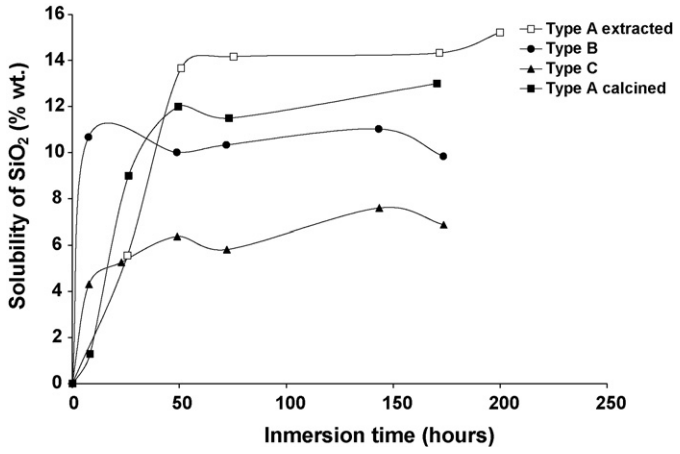

Fig. 4. Temporal evaluation of the amount of silicon released to SBF at 37 °C for the three kinds of silica synthesized in this work.

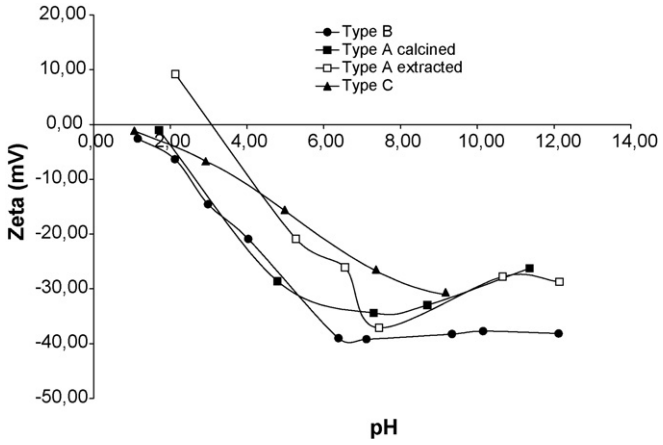

Fig. 6. Zeta potential of the different silica particles prepared in this work.

seen that the behaviour is rather similar, suggesting that the concentration of surface hydroxyl groups does not play an important role in accelerating the dissolution of silica.

3.5. Standard BSA adsorption assay

3.5.1. Non-specific protein-binding tests

The removal of particle from circulation by the mononuclear phagocyte system (MPS) begins with the adsorption of plasma proteins (i.e., opsonins including complement proteins and immunoglobulins) on the particle surface [32,33]. Therefore, we evaluated the non-specific binding capacity of the synthesized nanoparticles using serum albumin (the most abundant blood protein) as a model.

The total amount of bovine serum albumin (BSA) adsorbed onto bare silica nanoparticles is shown in Fig. 5. As it could be observed, with increasing pH, the amount of adsorbed BSA decreased significantly. The maximum adsorption occurred at pH 4.7, which corresponds to the isoelectric point (p*I*) of BSA [34]. A possible explanation of the pH effect on adsorption may be related to the surface charge of silica particles and BSA. The measured zeta potentials of all the particles synthesized in this work at different pH are shown in Fig. 6. As can be observed, in all cases the isoelectric point of the silica was reached at a pH around 2. Therefore, all the silica particles have a positive charge below pH 2.0 and a negative charge above this pH value (which increases in magnitude as the pH value is raised). The net charge of BSA also varies with pH, being positive or negative if pH is below or above pH 4.7, respectively. Thus, at pH 7.4 both BSA and silica particles have a net negative charge, which results in the decrease of BSA adsorption due to electrostatic repulsion. At pH 4.7, BSA shows zero net surface charge and the negative charge on the silica particles is smaller. Therefore, at this pH value the electrostatic effect is less pronounced resulting in a higher adsorption of BSA. Moreover, it was already reported that BSA has several isomeric forms at different pH media. At its isoelectric point, the protein has the maximum of α-helix content which results in a more compact state of BSA molecules which could also promote adsorption [34,35].

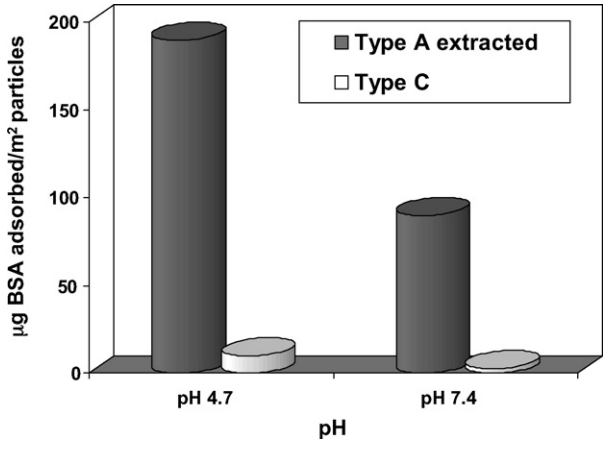

Fig. 5. Total amount of BSA adsorbed at different pH on bare (Type A extracted), and PEG(3000)-coated (Type C) silica nanoparticles. As Type C corresponds to dense silica particles the external area accessible to BSA adsorption corresponds to the total area measured by BET. In the case of Type A nanoparticles as they are mesoporous, the external area corresponds to the ~3% of the total area measured by nitrogen physisorption of surfactant-containing samples.

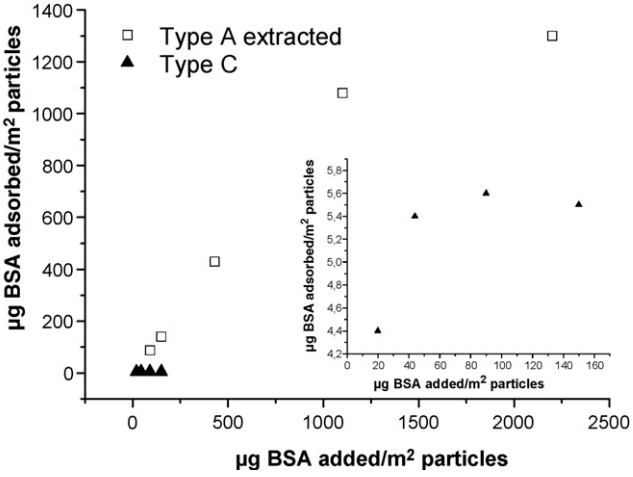

Fig. 7. Adsorbed BSA vs. BSA in solution (normalized per unit of surface area of the particles) to show the BSA adsorption capacity of bare (Type A extracted) and PEG(3000)-coated (Type C) silica nanoparticles.

3.5.2. Influence of PEGylation on the BSA adsorption

It is known that the presence of polymeric hydrophilic coatings increases the nanoparticle plasma half-life by minimizing the protein adsorption on their surfaces [36–38]. In Fig. 5, the adsorption of BSA on PEG(3000)-silica nanoparticles (Type C) at two different pH values (pH 4.7 that corresponds to pI of BSA and pH 7.4 which is the physiological pH value of blood) is also shown. From these results, it is clear that the presence of poly(ethylene glycol) on the surface of the silica nanoparticles significantly reduces BSA adsorption at both pH values. This could be attributed to the increased water-retaining capacity, charge neutrality and steric repulsion effects caused by PEG [39].

Fig. 7 shows the evolution of the amount of BSA adsorbed on bare and PEGylated nanoparticles as the load of BSA in the surrounding solution is increased. As can be seen, the maximum adsorbable amount of BSA under the conditions used can be calculated: 1300 μg of protein/m^2 (external surface) in the case of bare nanoparticles, an amount that is around 250 times lower for the case of PEG(3000)-modified silica.

It has been reported that the length and shape of the PEG chains could modify steric effects around the particles, inducing significant changes on protein adsorption [40–42]. The work of Xu et al. [25] showed that an increase in the PEG molecular weight from PEG 650 g/mol to PEG 6000 g/mol produced a decrease in the amount of protein adsorbed; however, the tendency shows asymptotic behaviour. Therefore, we evaluated the use of PEGs of different molecular weights in the synthesis of PEGylated silica nanoparticles. The use of PEG chains with a molecular weight higher than 3000 g/mol had little influence on BSA adsorption on the silica particles synthesized in this work (from 5.2 μg of protein/m^2 for the PEG(3000)-modified silica to 5.0 μg of protein/m^2 for the PEG(35,000)-modified silica). An optimal molecular weight of the PEG chain at 2000–5000 g/mol has also been described in the literature [43].

Protein adsorption could also be reduced by increasing the surface density of PEG chains grafted on the silica particles. To this end, the synthesis temperature was increased with the aim of accelerating the esterification reaction between the –OR groups of the TEOS and the PEG hydroxyl groups [25]. However, for the particles where the synthesis was carried out at the higher temperature (60 °C), the amount of BSA adsorbed (42 wt.% of the total BSA added was adsorbed) was much higher than for the PEG-modified particles synthesized at room temperature during the same contact time (11 wt.% of the total BSA adsorbed). This suggests that the higher synthesis temperature does not result in a higher surface density of PEG, possibly due to the acceleration of competing reactions. However, this issue is still under investigation in our laboratory.

Finally, some attempts were also carried out to coat PEG on previously synthesized Type A silica particles following the experimental procedure described by Alcantar et al. [44] which described the grafting of silica surfaces with polyethylenglycol using an ester bond. Our results (not shown) indicate that, while hydrogen bonding between PEG and silanol groups occurs, the stability of the bonding is poor both in a non-ionic detergent (Tween-20) and in a medium with high ionic force. In addition, this route seems less desirable, since particles with covalently bound PEG chains achieve longer blood circulation half-lives than similar particles with only surface adsorbed PEG [10].

4. Conclusions

Different synthesis parameters, including the concentration of the silica source (or the ratio silica source/water), the polarity and size of the alcohol, and the amount of the catalyst added, can be tuned in order to reduce the particle sizes of silica nanoparticles prepared by the sol–gel procedure. For the mesoporous silica particles, removal of the surfactant by extraction instead of calcination yields a higher concentration of surface hydroxyl groups; however, the procedure of surfactant removal does not seem to affect the solubility of silica particles which is very low in any case, even for the silica particles synthesized using surfactant-free procedures. Finally, the addition of PEG is effective as a stealthing procedure, as PEGylated silica particles show a considerably decreased protein adsorption compared to bare silica. The reduction of protein adsorption is fairly constant after increasing the PEG chain length to above 3000 g/mol.

Acknowledgements

Financial assistance from the Spanish Nanoscience and Nanotechnology Action NAN200409270-C3-1/2, the CIBER-BBN and the CSD2006-00012 Consolider Ingenio 2010 program for the support of this study are gratefully acknowledged. M. Arruebo would like to acknowledge the support from the 2006 "Ramón y Cajal" program (order ECI/158/2005).

References

[1] Z.P. Xu, Q.H. Zeng, G.Q. Lu, A.B. Yu, Inorganic nanoparticles as carriers for efficient cellular delivery, Chem. Eng. Sci. 61 (2006) 1027–1040.
[2] S.J. Son, X. Bai, A. Nan, H. Ghandehari, S.B. Lee, Template synthesis of multifunctional nanotubes for controlled release, J. Control. Release 114 (2006) 143–152.
[3] J. Livage, T. Coradin, C. Roux, Encapsulation of biomolecules in silica gels, J. Phys. Condes. Matter 13 (2001) R673–R691.
[4] S. Radin, G. El-Bassyouni, E.J. Vresilovic, E. Schepers, P. Ducheyne, In vivo tissue response to resorbable silica xerogels as controlled-release materials, Biomaterials 26 (2005) 1043–1052.
[5] P. Kortesuo, M. Ahola, S. Karlsson, I. Kangasniemi, A. Yli-Urpo, J. Kiesvaara, Silica xerogel as an implantable carrier for controlled drug delivery—evaluation of drug distribution and tissue effects after implantation, Biomaterials 21 (2000) 193–198.
[6] I. Roy, T.Y. Ohulchanskyy, H.E. Pudavar, E.J. Bergey, A.R. Oseroff, J. Morgan, T.J. Dougherty, P.N. Prasad, Ceramic-based nanoparticles entrapping water-insoluble photosensitizing anticancer drugs: a novel drug-carrier system for photodynamic therapy, J. Am. Chem. Soc. 125 (2003) 7860–7865.
[7] T.K. Jain, I. Roy, T.K. De, A. Maitra, Nanometer silica particles encapsulating active compounds: a novel ceramic drug carrier, J. Am. Chem. Soc. 120 (1998) 11092–11095.
[8] J.F. Díaz, K.J. Balkus, Enzyme immobilization in MCM-41 molecular sieve, J. Mol. Catal. B Enzymatic 2 (1996) 115–126.
[9] S.M. Moghimi, Mechanisms of splenic clearance of blood-cells and particles—towards development of new splenotropic agents, Adv. Drug Deliv. Rev. 17 (1995) 103–115.
[10] D.E. Owens, N.A. Peppas, Opsonization, biodistribution, and pharmacokinetics of polymeric nanoparticles, Int. J. Pharm. 307 (2006) 93–102.

[11] A. Gabizon, H. Shmeeda, A.T. Horowitz, S. Zalipsky, Tumor cell targeting of liposome-entrapped drugs with phospholipid-anchored folic acid–PEG conjugates, Adv. Drug Deliv. Rev. 56 (2004) 1177–1192.
[12] A. Bogdanov, S.C. Wright, E.M. Marecos, A. Bogdanova, C. Martin, P. Petherick, R. Weissleder, A long-circulating co-polymer in "passive targeting" to solid tumors, J. Drug Target 4 (1997) 321–327.
[13] S.K. Hobbs, W.L. Monsky, F. Yuan, W.G. Roberts, L. Griffith, V.P. Torchilin, R.K. Jain, Regulation of transport pathways in tumour vessels: role of tumour type and microenvironment, Proc. Natl. Acad. Sci. U.S.A. 98 (1998) 4607–4612.
[14] W. Stöber, A. Fink, E. Bohn, Controlled growth of monodisperse silica spheres in micron size range, J. Colloid Interface Sci. 26 (1968) 62–68.
[15] F. Balas, M. Rodríguez-Delgado, C. Otero-Arean, F. Conde, E. Matesanz, L. Esquivias, J. Ramírez-Castellanos, J. González-Calbet, M. Vallet-Regí, Structural characterization of nanosized silica spheres, Solid State Sci. 9 (2007) 351–356.
[16] S. Tabatabaei, A. Shukohfar, R. Aghababazadeh, A. Mirhabibi, Experimental study of the synthesis and characterisation of silica nanoparticles via the sol–gel method, J. Phys.: Conf. Ser. 26 (2006) 371–374.
[17] C.E. Fowler, D. Khushalani, B. Lebeau, S. Mann, Nanoscale materials with mesostructured interiors, Adv. Mater. 13 (2001) 649–652.
[18] G.J. Soler-Illia, Clement Sánchez, B. Lebeau, J Patarin, Chemical strategies to design textured materials: from microporous and mesoporous oxides to nanonetworks and hierarchical structures, Chem. Rev. 102 (2002) 4093–4138;
R.D. Badley, W.T. Ford, F.J. Mcenroe, R.A. Assink, Surface modification of colloidal silica, Langmuir 6 (1990) 792–801.
[19] G. Tolnai, F. Csempesz, M. Kabai-Faix, E. Kalman, Z. Keresztes, A.L. Kovacs, J.J. Ramsden, Z. Horvolgyi, Preparation and characterization of surface-modified silica-nanoparticles, Langmuir 17 (2001) 2683–2687.
[20] L. Huang, Z. Wang, J. Sun, L. Miao, Q. Li, Y. Yan, D. Zhao, Fabrication of ordered porous structures by self-assembly of zeolite nanocrystals, J. Am. Chem. Soc. 122 (2000) 3530–3531.
[21] S.K. Parida, S. Dash, S. Patel, B.K. Mishra, Adsorption of organic molecules on silica surface, Adv. Colloid Interface Sci. 121 (2006) 77–110.
[22] F. Li, Z. Wang, A. Stein, Shaping mesoporous silica nanoparticles by disassembly of hierarchically porous structures, Angew. Chem. Int. Edit. 46 (2007) 1885–1888.
[23] W. Zeng, X.F. Qian, Y.B. Zhang, J. Yin, Z.K. Zhu, Organic modified mesoporous MCM-41 through solvothermal process as drug delivery system, Mater. Res. Bull. 40 (2005) 766–772.
[24] O.I. Lebedev, G. Van Tendeloo, O. Collart, P. Cool, E.F. Vansant, Structure and microstructure of nanoscale mesoporous silica spheres, Solid State Sci. 6 (2004) 489–498.
[25] H. Xu, F. Yan, E.C. Monson, R. Kopelman, Room-temperature preparation and characterization of poly (ethylene glycol)-coated silica nanoparticles for biomedical applications, J. Biomed. Mater. Res. Part A 66A (2003) 870–879.
[26] T. Kokubo, H. Kushitani, S. Sakka, T. Kitsugi, T. Yamamuro, Solutions able to reproduce in vivo surface-structure changes in bioactive glass-ceramic A-W3, J. Biomed. Mater. Res. 24 (1990) 721–734.
[27] P.K. Smith, R.I. Krohn, G.F. Hermanson, A.K. Mallia, F.H. Gartner, M.D. Provenzano, E.K. Fujimoto, N.M. Goeke, D.C. Olson, D.C. Klent, Measurement of protein using bicinchoninic acid, Anal. Biochem. 150 (1985) 76–82.
[28] R. Duncan, S. Gac-Breton, R. Keane, R. Musila, Y.N. Sat, R. Satchi, F. Searle, Polymer–drug conjugates, PDEPT and PELT: basic principles for design and transfer from the laboratory to clinic, J. Control. Release 74 (2001) 135–146.
[29] Y.H. Deng, C.C. Wang, J.H. Hu, W.L. Yang, S.K. Fu, Investigation of formation of silica-coated magnetite nanoparticles via sol–gel approach, Colloid Surf. A Physicochem. Eng. Asp. 262 (2005) 87–93.
[30] R. Vacassy, R.J. Flatt, H. Hofmann, K.S. Choi, R.K. Singh, Synthesis of microporous silica spheres, J. Colloid Interface Sci. 227 (2000) 302–315.
[31] W.L. Lindsay, Chemical Equilibria in Soil, John Wiley & Sons, USA, 1979.
[32] T. Neuberger, B. Schöpf, H. Hofmann, M. Hofmann, B. von Rechenberg, Superparamagnetic nanoparticles for biomedical applications: possibilities and limitations of a new drug delivery system, J. Magn. Magn. Mater. 293 (2005) 483–496.
[33] E. Duguet, S. Vasseur, S. Mornet, J.M. Devoisselle, Magnetic nanoparticles and their applications in medicine, Nanomedical 1 (2006) 157–168.
[34] T. Peters Jr., Serum albumin, Adv. Protein Chem. 37 (1985) 161–245.
[35] Z.G. Peng, K. Hidajat, M.S. Uddin, Adsorption of bovine serum albumin on nanosized magnetic particles, J. Colloid Interface Sci. 271 (2004) 277–283.
[36] R. Michel, S. Pasche, M. Textor, D.G. Castner, Influence of PEG architecture on protein adsorption and conformation, Langmuir 21 (2005) 12327–12332.
[37] A.K. Gupta, M. Gupta, Synthesis and surface engineering of iron oxide nanoparticles for biomedical applications, Biomaterials 26 (2005) 3995–4021.
[38] S.W. Choi, W.S. Kim, J.H. Kim, Surface modification of functional nanoparticles for controlled drug delivery, J. Dispersion Sci. Technol. 24 (2003) 475–487.
[39] J. Andrade, V. Hlady, A.P. Wei, C.H. Ho, A. Laea, S.Y. Jeon, E. Dtraup, Proteins at interfaces: principles, multivariate aspects, protein resistant surfaces, and direct imaging and manipulation of adsorbed proteins, J. Clin. Mater. 11 (1–4) (1992) 67–84.
[40] R. Gref, M. Luck, M. Quellec, M. Marchand, E. Dellacherie, S. Harnisch, T. Blunk, R.H. Muller, Stealth corona-core nanoparticles surface modified by polyethylene glycol (PEG): influences of the corona (PEG chain length and surface density) and of the core composition on phagocytic uptake and plasma protein adsorption, Colloid Surf. B Biointerfaces 18 (2000) 301–313.
[41] S. Pasche, J. Voros, H.J. Griesser, N. Spencer, M. Tector, Effects of ionic strength and surface charge on protein adsorption at PEGylated surfaces, J. Phys. Chem. B 109 (2005) 17545–17552.
[42] A. Vonarbourg, C. Passirani, P. Saulnier, J.P. Benoit, Parameters influencing the stealthiness of colloidal drug delivery systems, Biomaterials 27 (2006) 4356–4373.
[43] M.T. Peracchia, Stealth nanoparticles for intravenous administration, STP Pharma Sci. 13 (2003) 155–161.
[44] N.A. Alcantar, E.S. Aydil, J.N. Israelachvili, Polyethylene glycol-coated biocompatible surfaces, J. Biomed. Mater. Res. 51 (2000) 343–351.